Nanoscale

ROYAL SOCIETY OF CHEMISTRY

COMMUNICATION

View Article Online
View Journal | View Issue

Check for updates

Cite this: *Nanoscale*, 2025, **17**, 17033

Received 14th February 2025,
Accepted 24th June 2025

DOI: 10.1039/d5nr00657k

rsc.li/nanoscale

Published on 25 June 2025. Downloaded on 3/2/2026 11:28:34 PM.

Investigation of the oxygen ligand hole of Ni-rich layered cathodes: a new organic coating for enhancing battery performance †

Fu-Ming Wang, *[a,b,c,d] Laurien Merinda,[a] Nan-Hung Yeh,[a] Rio Akbar Yuwono,[a] Hao-Hsuan Hsia,[a] Chusnul Khotimah[a] and Nae-Lih Wu [e,f]

Ni-rich (Ni content > 60%) layered cathodes are currently the most promising materials for lithium-ion batteries due to their high capacity and elevated voltage plateau compared to $LiFePO_4$. However, Ni-rich cathodes face significant challenges, such as Jahn–Teller distortion, cation mixing, electrolyte deprotonation, and the presence of residual lithium compounds. These issues impede the widespread use of high-energy-density lithium-ion batteries employing Ni-rich cathodes. Ni-rich cathodes, containing a high concentration of Ni^{3+}, encounter another problem known as the oxygen ligand hole effect, which affects the hybridization of O 2p and Ni 3d orbitals. Anionic redox occurs at the oxygen site with Ni^{3+}, leading to a decrease in electron density, making the formation of Ni^{4+} at high states of charge (SOC) difficult. Consequently, battery capacity is primarily derived from anionic redox reactions. This study presents an organic coating (OC) designed to enhance the stability of the oxygen ligand hole, enabling greater capacity through enhanced Li^+ interaction. Additionally, Ni-rich cathodes often suffer from gas evolution when charged to a high SOC, primarily due to the instability of the Ni–O bond. The OC is hypothesized to support the chemical reduction of Ni $2p^5 3d^{n+2}\underline{L}$ back to Ni $2p^6 3d^{n+1}\underline{L}$, where the $\underline{L}$ represents O $1s^1 2p^{x+1} \rightarrow$ O $1s^2 2p^x$ on the surface of NMC811, thereby strengthening the oxygen ligand hole and stabilizing covalent Ni^{3+}. This improvement results in the OC-modified NMC811 exhibiting outstanding cycle performance under high-rate tests and excellent stability at high temperatures.

Introduction

Lithium-ion batteries (LIBs) have been under development for over 30 years since their commercial introduction by Sony in 1991. The first successful and widely adopted cathode material was $LiCoO_2$ (LCO), developed by Prof. Goodenough in 1980, which earned him the Nobel Prize in Chemistry in 2019. The rapid growth in markets such as portable electronics, electric vehicles (EVs), and energy storage has drastically increased the demand for LIBs in recent years. Ni-rich (Ni content > 60%) layered cathodes are now being used as alternatives to LCO to provide higher energy density at lower cost. However, issues such as cation mixing,[1–3] residual lithium compounds,[4,5] carbonate deprotonation,[6–9] and Jahn–Teller distortion[10,11] have limited the use of Ni-rich layered compounds. Efforts to overcome these issues include coating inert substances on the active material's surface,[12,13] doping with other transition metals,[14,15] using ceramic separators to prevent electrolyte decomposition,[16,17] and precisely controlling the charge profile to avoid side reactions like H2–H3 transition.[18]

Another significant issue, which is often overlooked, is the oxygen ligand hole effect from the Ni–O hybridization orbital in Ni-rich layered compounds.[19–21] Over two decades ago, Uchimoto and Kim *et al.* used X-ray absorption spectroscopy (XAS) to study $Li_yNi_{1-x}Al_xO_2$[19] and $LiNiO_2$ (LNO),[20] revealing that the mixing of O 2p and Ni 3d orbitals profoundly impacts the electrochemical reaction during lithiation and delithiation. For example, Uchimoto *et al.* found that the intensity of the e_g band of the Ni L3 edge increases when increasing the delithiated state of LNO, whereby the valence of the Ni ion approaches that of Ni^{3+}. In the meantime, the O 1s spectrum presents a variation at 528 eV where the peak intensity is increased by increasing the delithiated state of LNO.[19] They explained that the delithiation of LNO affects the O 2p orbital

[a]*Graduate Institute of Applied Science and Technology, National Taiwan University of Science and Technology, Taipei, Taiwan. E-mail: mccabe@mail.ntust.edu.tw*
[b]*Sustainable Energy Center, National Taiwan University of Science and Technology, Taipei, Taiwan*
[c]*Department of Chemical Engineering, Chung Yuan Christian University, Taoyuan, Taiwan*
[d]*R&D Center for Membrane Technology, Chung Yuan Christian University, Taoyuan, Taiwan*
[e]*Department of Chemical Engineering, National Taiwan University, Taipei, 10617, Taiwan*
[f]*Advanced Research Center for Green Materials Science and Technology, National Taiwan University, Taipei, 10617, Taiwan*

† Electronic supplementary information (ESI) available. See DOI: https://doi.org/10.1039/d5nr00657k

Published on 25 June 2025. Downloaded on 3/2/2026 11:28:34 PM.

not involving Ni. Meanwhile, Kim *et al.* observed that Li substitution in Ni-rich compounds leads to hole formation in the O 2p orbital, as opposed to the Ni 3d orbital. This situation results in a final hybridization of $O1s^1\underline{c}$ + $Ni3d^7$ ($t2g^6e_g^1$), where the $\underline{c}$ is the O 1s electron to the hole state in the O 2p level. Therefore, the electronic configuration of the Ni ion in the delithiated Ni-rich compounds can be proposed to be $3d^7$ (Ni^{2+}) and $3d^8\underline{L}$ (Ni^{III} not Ni^{3+}), where the $\underline{L}$ represents the hole in the O 2p orbital.

More recently, Zhang *et al.* used LNO as a catalyst for the oxygen evolution reaction (OER) and found that delithiated LNO significantly promotes the formation of $3d^8\underline{L}^2$ (double ligand–hole state) from the oxidation of $3d^8\underline{L}$, resulting in high OER activity through a lattice oxygen oxidation mechanism.[22] To achieve Norskov's model (four-electron process),[23] the intermediates such as *OH, *O, and *OOH in the OER reaction need to bind on the surface of the catalysts by adsorption to perform oxygen evolution; the most common efficient precious metal-based electro-catalysts are IrO_2 and RuO_2. Zhang demonstrated that delithiated LNO (53 mV dec^{-1}) exhibits faster reaction kinetics for the OER compared with IrO_2 (54 mV dec^{-1}), NiOOH (96 mV dec^{-1}), and C (131 mV dec^{-1}), while also decreasing the over potential of the OER.[22] They also claim that delithiaed LNO can produce 75% $3d^8\underline{L}^2$ and 25% $3d^8\underline{L}$ for an average $Ni^{3.75+}$ valence state after the OER in KOH aqueous solution, although in the LIB field it is known that it is not easy to maintain a high oxidation state of LNO in aqueous solution.[22,23] Furthermore, they also compared their LNO with four other LNO samples from the literature to demonstrate the absence of Ni^{2+} impurities. However, they did not discuss the effects of the Ni^{2+} in LNO on the oxygen ligand hole or the catalytic performance.

Although several studies have investigated the effects of the oxygen ligand hole on the intrinsic properties of LNO and the OER catalyst performance, there has been no discussion of the effect of the oxygen ligand hole on the interfacial reaction in LIB.

In this research, a new organic coating (OC) is synthesized and its effects on the oxygen ligand hole of Ni-rich compounds are investigated. The results show that the OC stabilizes the high valence state of Ni ion at high temperature and provides high cycle retention for batteries.

Experiment

Synthesis of BU

Bismaleimide (Acros Organics, 97%) and uracil (Acros Organics, 99%) were mixed in *N*-methyl-2-pyrrolidinone (NMP, Acros Organics, 99%) under continuous stirring in an oil bath at 130 °C for 30 minutes. The solid content of the resulting BU solution was optimized to 7 wt%. The solution was stored in a refrigerator to prevent thermal or self-polymerization before reaction with Ni-rich layered materials ($LiNi_{0.8}Mn_{0.1}Co_{0.1}O_2$, NMC811; $LiNi_{0.6}Mn_{0.2}Co_{0.2}O_2$, NMC622). The BU structure and its material characterization based on NMR and FTIR are described in detail in the ESI (Fig. S1 and S2).†

Electrode preparation

In this study, NMC811 or NMC622 served as the cathode materials, with Li foil as the reference electrode, a polypropylene microporous film (Celgard 2320) as the separator, Super-P (SP) (Timcal) as the conductive agent, and polyvinylidene difluoride (PVDF) as the binder. All chemicals were used as received in a glove box. The NMC811 and NMC622 electrodes were fabricated by preparing a slurry of 90 wt% NMC811 or NMC622, 5 wt% SP, and 5 wt% PVDF in NMP solvent. The slurry was coated onto Al foil, dried at 110 °C for 2 h, and punched into 12 mm-diameter disks for half-cell tests. BU was added to the slurry at 1 wt% based on the mass of NMC811 or NMC622, and the reaction was allowed to proceed for 3 h at room temperature, ensuring that the surface of the NMC811 or NMC622 was uniformly covered with BU. The average area capacity of the electrodes was controlled to 3.5 mAh cm^{-2}.

Electrolyte preparation

An electrolyte was prepared with 1 M lithium hexafluorophosphate ($LiPF_6$) in ethylene carbonate (EC) and ethyl methyl carbonate (EMC) (1 : 2 volume ratio, battery grade, water content less than 20 ppm), purchased from Uni-onward Company, Taiwan. The battery fabrication and electrolyte preparation were performed in an Ar gas atmosphere inside a glove box to avoid moisture contamination.

Electrochemical performance

To investigate the electrochemical behaviour, CR2032-type coin cells were used. Charge and discharge were measured using a BAT-750B Battery Automatic Tester at a constant current of 0.1 C, between 2.8 and 4.3 V *vs.* Li/Li^+, with a constant voltage charge of 4.3 V when the current dropped below 0.01 C. Cycle performance was tested at 0.1 C/0.1 C for the first three cycles at room temperature, followed by 0.5 C/0.5 C, 1 C/1 C, and 1 C/2 C for 200 cycles at 60 °C.

Effect of electronic configuration on synchrotron radiation

In situ electronic structure analysis of the electrodes (after disassembly in the glove box) was performed using synchrotron hard X-ray absorption spectroscopy (XAS). The hard XAS was performed in beamlines BL01C1, 17C1, and 20A1 at the National Synchrotron Radiation Research Center (NSRRC), Hsinchu, Taiwan. The hard XAS beamline covered the spectral range 5–40 keV, with an average energy-resolving power of 5 keV. The soft XAS beamline covered the spectral range 60–1250 eV, also with an average energy-resolving power of 60 eV. The end station was primarily designed for studying condensed-phase photochemistry and the electronic structures of new materials. *In situ* experiments were performed at C/10 in a modified coin cell. A Si (111) monochromatic double crystal was used to perform the energy scan, in which the parallelism was adjusted to eliminate high-order harmonics. All spectra were obtained in transmission mode. Ionization chambers were used as detectors to monitor the intensity of the incident beams on, and transmitted beams through, the specimen,

 This journal is © The Royal Society of Chemistry 2025

Published on 25 June 2025. Downloaded on 3/2/2026 11:28:34 PM.

enabling calculation of the absorption coefficient from the logarithm of the intensity ratio of the incident and transmitted beams.

Results and discussion

The electronic structure of the two NMC811 materials is measured using total electron yield soft X-ray absorption spectra (sXAS) at the O K edge. Winter *et al.* discussed the phenomenon observed in Ni-rich layered compounds, where the number of ligand holes in the O 2p orbital decreases with the discharge capacity of these materials.[21] Through investigations of ligand field energy and sXAS analysis, they calculated that for all layered cathode materials (NMC111, NMC622, NMC811) charged to 100% state of charge (SOC), the electronic structure of Ni exhibits an approximately 96% covalent character of Ni^{3+}, with the ligand hole displaying the highest intensity.

Upon discharge, the covalent Ni^{3+} content drops to 58–69%, while the ionic Ni^{2+} increases to 42–31%.[22,23] Notably, the ligand hole stabilizes with Ni^{3+} due to its negative charge-transfer energy regime, also known as ligand-to-metal charge transfer (LMCT). This confirms that the capacity delivered from Ni-rich layered cathodes is governed by anionic redox at high SOC ranges.[21] The oxygen site associated with Ni^{3+} lowers its electron density and undergoes a redox reaction: $O^{2-} \Leftrightarrow O^{(-2+x)-} + xe^{-}$ $(0 < x < 1)$,[21] which is further supported by the sXAS results.[19,20] Consequently, Ni^{4+} formation at high SOC is unlikely due to the characteristics of the ligand hole. Furthermore, the chemical equilibrium of the Ni configuration can be described as Ni $3d^{x} \Leftrightarrow$ Ni $3d^{x+1}\underline{L}$, indicating that both Ni and O are the primary redox-active elements in Ni-rich compounds when the ratio of [Ni $3d^{x+1}\underline{L}$]/[Ni $3d^{x}$ + Ni $3d^{x+1}$ $\underline{L}$] is 0.5. The capacity of Ni-rich layered compounds is thus delivered by ionic Ni^{2+} in low SOC ranges. In summary, Ni–O hybridization induces the electrochemical oxidation process Ni $2p^{6}3d^{n+1}\underline{L} \rightarrow$ Ni $2p^{5}3d^{n+2}\underline{L}$, where the $\underline{L}$ represents O $1s^{2}2p^{x} \rightarrow$ O $1s^{1}2p^{x+1}$.[22,23] Based on their observations, the peak at 528 eV is attributed to the oxygen ligand hole with covalent Ni^{3+} (hybridization), while the peak at 529 eV corresponds to the TM 3d–O 2p orbital.

Fig. 1a shows that pristine NMC811 exhibits a clear plateau between 528 and 529 eV, which may separate into two equally intense peaks, indicating an equal concentration of oxygen ligand holes (528 eV) and TM 3d–O 2p orbitals (529 eV).

Additionally, lithium residue compounds (Li_2CO_3 and LiOH) are found on the pristine NMC811 surface (~533 eV), suggesting that lattice oxygen is spontaneously oxidized, releasing lithium ions that further react with CO_2 and H_2O.[4,24] This reaction decreases the number of oxygen ligand holes due to the formation of Ni^{2+} (Ni^{2+}–O found at 531.7 eV), which in turn induces cation mixing in the electrochemical reaction.[25–27] Compared to fresh NMC811, the 528 eV peak shows higher intensity than the of the 529 eV peak, indicating a greater proportion of Ni^{3+} relative to Ni^{2+}, Co^{3+}, and Mn^{4+}.[28,29] Interestingly, the OC mixed with NMC811 significantly increases the number of oxygen ligand holes, reinforcing the presence of covalent Ni^{3+}. Additionally, lithium residue compounds are reduced, as indicated by the lower strength of Ni^{2+}–O at 531.3 eV (inset of Fig. 1a). Previous discussion had illustrated that adequate oxygen concentration during the synthesis process helps to maintain the presence of covalent Ni^{3+}.[1] Thus, the increase in oxygen ligand holes due to OC addition significantly alters the surface chemical composition of NMC811. The oxygen ligand hole after OC addition is defined as the oxygen 1s electron to the hole state in the oxygen 2p level, represented by the formula O $1s^{2}2p^{x} \rightarrow$ O $1s^{1}2p^{x+1}$. From the OC structure shown in Scheme 1, it is notable that OC contains several carbonyl (C═O) groups, which undergo catalytic conversion to C–OH group *via* hydride anion transfer. The C–OH groups may dissociate into C–O* while releasing electrons (C–OH → C–O* + H^{+} + e^{-}). Two possible reactions are proposed: first, the released protons lower the solution's pH, facilitating the decomposition of lithium residue compounds, and second, C–O* captures Li^{+}, forming C–OLi bonds, known as lithiated OC (LiOC). Additionally, electrons released from C–OH reduction may occupy unoccupied orbitals. Consequently, during the transformation from C–OH to C–OLi, Ni $2p^{5}3d^{n+2}\underline{L}$ is chemically reduced back to Ni $2p^{6}3d^{n+2}\underline{L}$, with L representing the surface transition Ni $2p^{5}3d^{n+2}\underline{L}$ in OC NMC811, thereby strengthening the oxygen ligand hole associated with covalent Ni^{3+}, and in agreement with published results.[24,30,31]

Fig. 1b presents the sXAS spectra at the Ni K edge for two different as-prepared NMC811 electrodes. The two peaks corresponding to the t_{2g} and e_g bands in the L3 edge region are evident. A notable feature of OC NMC811 is that the e_g band is 0.25 eV higher than that of pristine NMC811. Literature suggests that changes in Ni's electronic state arise from variations in unoccupied Ni $d_{x^2-y^2}$ (high energy, in-plane) and d_{3z2-r2} (lower energy, out-of-plane) states.[32] The energy difference ($\Delta e_g \sim 0.25$ eV) between these orbitals indicates that higher electron occupancy in the Ni $d_{x^2-y^2}$ orbital enhances the covalent Ni^{3+} oxygen ligand hole due to LiOC formation on the NMC811 surface.

Fig. 1c shows the effects of temperature on the sXAS spectra at the Ni K edge for two fully charged (100% SOC) NMC811 electrodes. The dashed line represents electrodes measured at 300 K. The t_{2g} band intensity of pristine NMC811 is significantly lower than that of OC NMC811, indicating that OC enhances the electrochemical oxidation of Ni^{2+} and supports the anionic redox process. Increased oxidation of Ni^{2+} to a higher valence state suggests improved battery capacity. Furthermore, the e_g band energy of OC NMC811 is slightly (~0.1 eV) higher than that of pristine NMC811, indicating similar Ni $d_{x^2-y^2}$ and $d_{3z^2-r^2}$ orbital energy levels at 100% SOC. When heated to 660 K, the two electrodes exhibit distinct behaviours. Ni-rich layered compounds are known to be highly unstable at 100% SOC due to oxygen evolution from Ni 3d–O 2p bond instability,[18,24,33] electrolyte decomposition *via* deprotonation,[6] and Jahn–Teller distortion.[34] These effects lead to gas evolution, structural collapse, and increased impedance,

Published on 25 June 2025. Downloaded on 3/2/2026 11:28:34 PM.

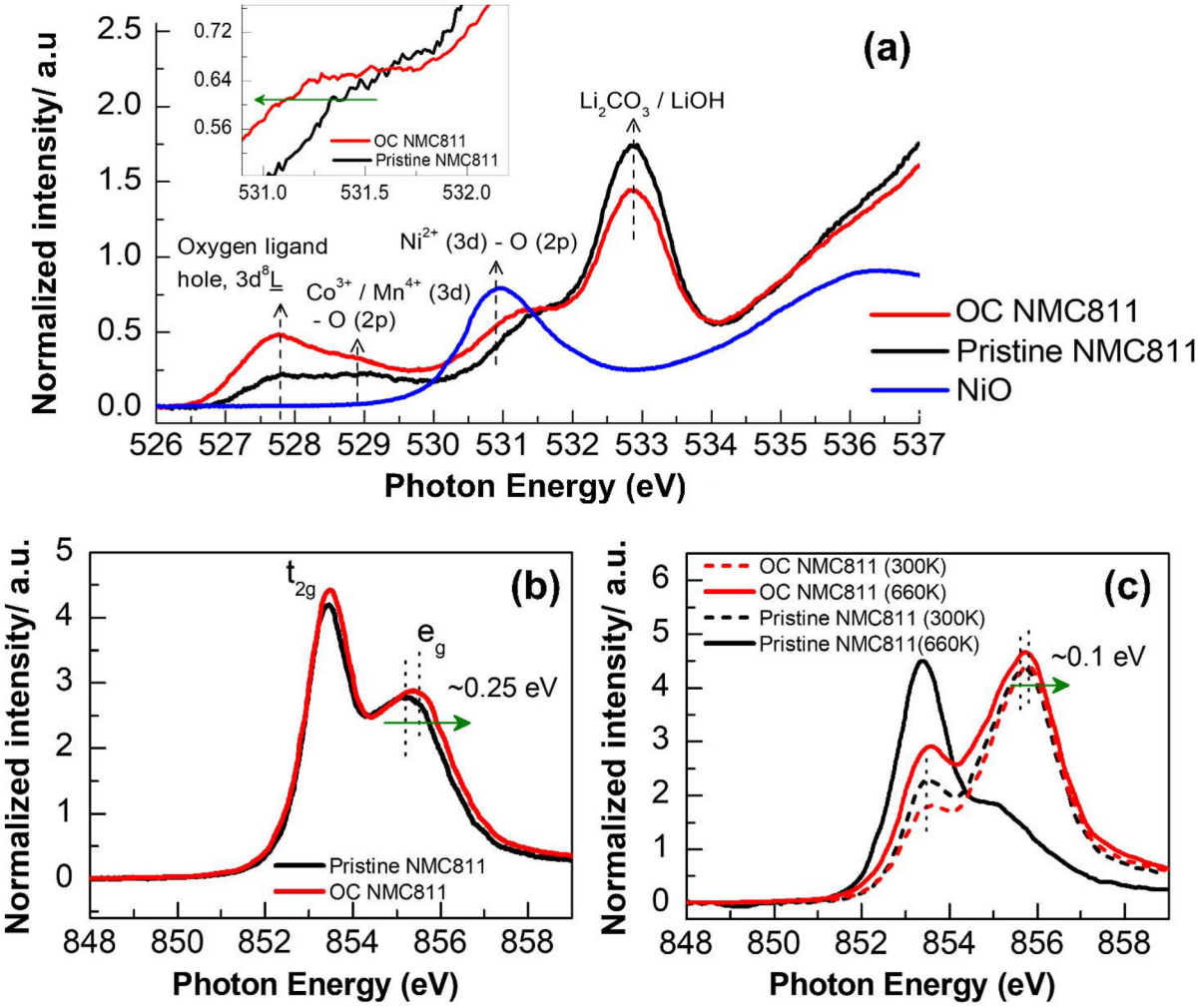

Fig. 1 sXAS spectra of the as-prepared NMC811 electrodes for (a) O K edge and (b) Ni K edge, and (c) *in situ* Ni K edge of the fully charged NMC811 electrode.

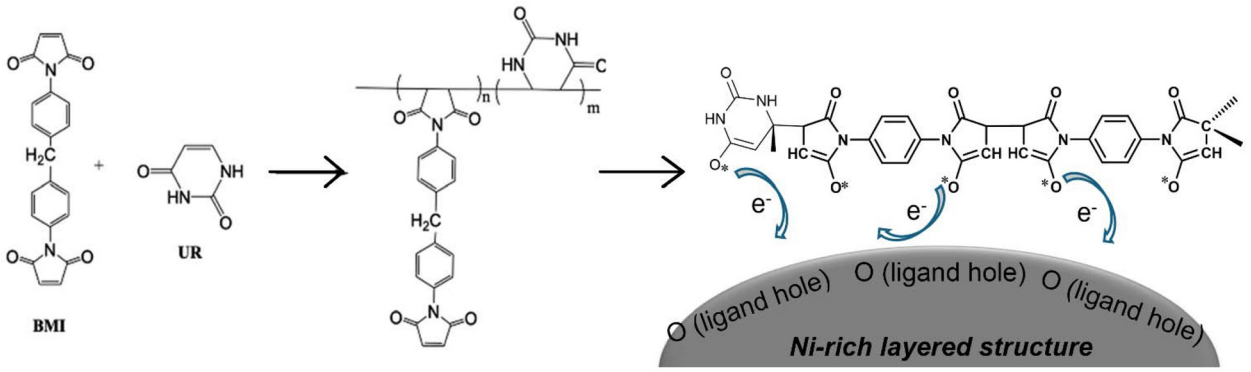

Scheme 1 . Schematic representation of organic coating and its interaction on the surface of Ni-rich layered cathodes.

ultimately reducing battery lifespan and posing safety risks. To mitigate these issues, Ni-rich layered compounds should not be fully charged or exposed to high temperatures without a precise battery management system. Fig. 1c demonstrates that the e_g band of OC NMC811 remains stable at high temperatures, consistent with the findings for NMC622,[24] where oxygen release is significantly reduced by stabilizing the anionic redox at high SOC.

 This journal is © The Royal Society of Chemistry 2025

Published on 25 June 2025. Downloaded on 3/2/2026 11:28:34 PM.

Fig. 2a presents the *in situ* EXAFS results for two NMC811 electrodes, showing distinct Ni–O bond lengths in pristine NMC811 (~1.902 Å and ~2.086 Å). According to Jahn–Teller distortion theory, four short and two long bonds characterize the low-spin Ni^{3+} $(t_{2g})^6(e_g)^1$ configuration in an octahedral $[NiO_6]$ crystal. During charging, Ni–O bonds systematically shorten, with increased intensity of short Ni–O bonds due to Ni^{3+}–O covalent bonding. Upon discharging to 2.8 V, the Ni–O bond length remains shorter than the bond length at the initial open-circuit voltage (OCV), indicating an irreversible reaction and loss of Li^+ in the H2–H3 formation range. In contrast, Fig. 2b shows that the OC NMC811 also exhibits four short (~1.902 Å) and two long (~2.086 Å) bonds, indicating that the OC does not affect the Ni–O when it covers the surface. By increment of the voltage, the short Ni–O bond length instantaneously increases from 3.95 V and reaches the maximum intensity at 4.15 V and then stays the same at 4.3 V. In the meantime, there is no difference in the length at the OCV and 2.8 V. These results indicate that the OC prompts the ligand hole of Ni^{3+}–O covalent bond and allows more Li^+ join the redox reaction of battery. In fact, Fig. 3a states the different on discharging curves of two NMC811 electrodes is presented at 4.15 V. At this voltage, the OC NMC811 displays a better capacity (221.5 mAh g^{-1}) and than the pristine

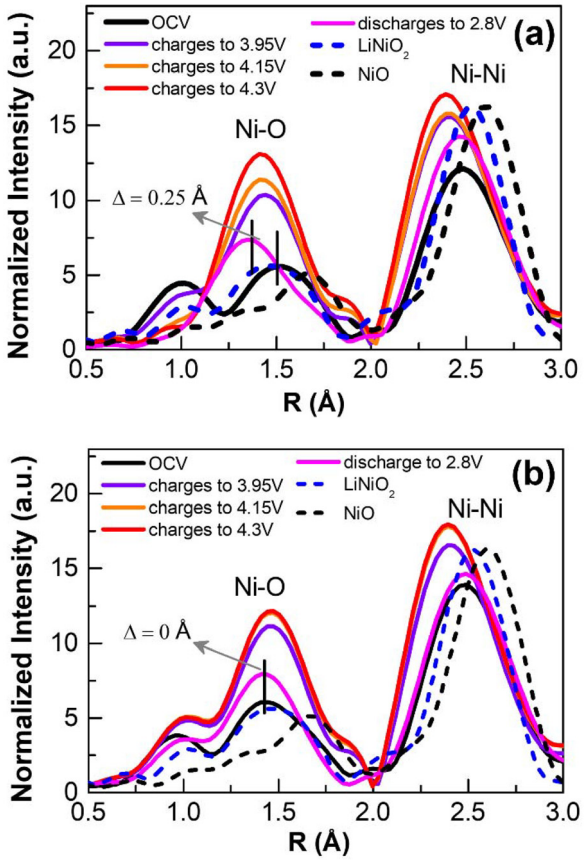

Fig. 2 *In situ* EXAFS spectra for (a) pristine NMC811 and (b) OC NMC811.

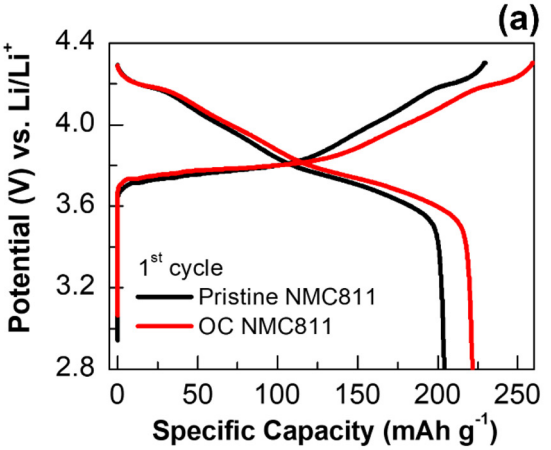

	Pristine NMC811	OC NMC811
Charge/ mAh g^{-1}	228.9	259.5
Discharge/ mAh g^{-1}	203.9	221.5
CE/ %	89.0	85.3

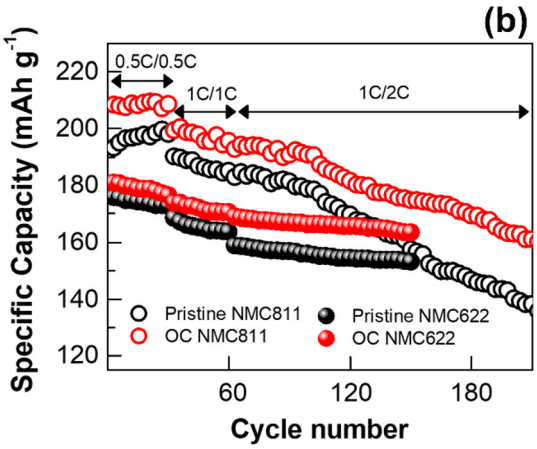

Fig. 3 Electrochemical performance of two NMC811 materials: (a) initial charge–discharge profile (0.1 C/0.1 C) at room temperature and (b) cycle retention at 60 °C.

(203.9 mAh g^{-1}). Fig. 3b shows the cycle performance of two NMC811 and two NMC622 electrodes tested at different rates. The dQ/dV shown in Fig. S3† clearly indicates that the OC@NMC811 stabilizes the H2–H3 phase compared with the pristine NMC811. In addition, the *operando* GC-MS results in Fig. S4† indicate that the gas evolution from NMC811 is significantly reduced. Fig. S5† shows the XPS analysis results for two fresh and cycled electrodes. The results demonstrate that the OC mitigates the formation of residual lithium compounds by reacting with surface lithium residues in the fresh state and the fluorine species are reduced in the OC NMC811 electrode after cycling. According to these results, the OC-modified electrodes deliver outstanding cycle retention and stability for the life test, indicating that the OC-reinforced oxygen ligand hole of the Ni^{3+} covalent band reliably maintains the electrochemical redox reaction for 200 cycles at 60 °C. Furthermore,

Published on 25 June 2025. Downloaded on 3/2/2026 11:28:34 PM.

the oxygen ligand hole may exhibit magnetic behaviour due to the low-spin Ni^{3+} state,[35] suggesting that the improvement in battery performance by the OC may also be influenced by magnetic effects.[36]

Conclusion

This study demonstrates the critical role of the oxygen ligand hole in Ni-rich cathodes for capacity delivery *via* anionic redox reactions. The stability of the oxygen ligand hole is often compromised by side reactions, such as gas evolution and the formation of residual lithium compounds. These issues cause surface impedance and structural collapse, leading to rapid performance degradation. To overcome these challenges, a new organic coating (OC) was developed to stabilize the oxygen ligand hole in the hybridization of O 2p and Ni 3d orbitals, enabling enhanced capacity, cycle retention, and high-temperature performance. The results show that the OC significantly improves battery performance by reinforcing the interaction between the oxygen ligand holes and Li^+, demonstrating its potential for advancing the application of Ni-rich cathodes in high-performance LIBs. This work shows that maintaining the oxygen ligand hole of Ni-rich cathodes by a suitable method is essential, and OC is an outstanding candidate for overcoming these drawbacks.

Author contributions

Prof. Fu-Ming Wang analysed the data and wrote this manuscript. In addition, he handled the project and designed all experiments. Laurien Merinda performed additional experiments. Dr Nan-Hung Yeh performed those experiments during his PhD program. Dr Rio Akbar Yuwono investigated and validated the data for the ESI.† Hao-Hsuan Hsia performed the *operando* GC-MS analysis for the material characterization data for the ESI.† Dr Chusnul Khotimah helped to edit the figures and format this submission. Prof. Nae-Lih Wu handled the project and managed the resources.

Conflicts of interest

There are no conflicts to declare.

Data availability

Data for this article are available upon reasonable request.

Acknowledgements

The authors are grateful for the financial support from the National Science and Technology Council (NSTC) and the Ministry of Education (MOE), "Sustainable Electrochemical Energy Development Center" (SEED) project of Taiwan, R.O.C., under grant numbers 112-2923-E-007-005, 112-2622-E-011-026, 112-2221-E-011-013-MY3, 113-2811-E-011-034-MY2, 113-2923-E-007-015, and 113-2622-8-01-011-.

References

1 R. A. Yuwono, F.-M. Wang, N.-L. Wu, Y.-C. Chen, H. Chen, J.-M. Chen, S.-C. Haw, J.-F. Lee, R.-K. Xie, H.-S. Sheu, P.-Y. Chang, C. Khotimah, L. Merinda and R. Hsing, *Chem. Eng. J.*, 2023, **456**, 141065.
2 F. Fan, R. Zheng, T. Zeng, H. Xu, X. Wen, X. Wang, G. Tian, S. Wang, C. Zeng, W. Xiang and C. Shu, *Chem. Eng. J.*, 2023, **477**, 147181.
3 J. Li, G. Liang, W. Zheng, S. Zhang, K. Davey, W. K. Pang and Z. Guo, *Nano Mater. Sci.*, 2023, **5**, 404–420.
4 R. A. Yuwono, C. Khotimah, F.-M. Wang, N.-L. Wu, A. C. Imawan, R. Foeng, P.-C. Huang, G.-Y. Liu, S.-C. Haw and H.-S. Sheu, *J. Energy Storage*, 2024, **92**, 112184.
5 J. Park, Y. Kim, Y. Kim, J. Park, D. G. Lee, Y. Lee, J. Hwang, K.-Y. Park and D. Lee, *Chem. Eng. J.*, 2023, **467**, 143335.
6 L. Merinda, F.-M. Wang, N.-L. Wu, R. A. Yuwono, C. Khotimah, U. Qonita, W.-H. Huang, P.-W. Tiong, C.-K. Chang, P.-H. Hsu, C.-W. Pao, J.-L. Chen, C.-L. Chen and T.-S. Chan, *J. Mater. Chem. A*, 2024, **12**, 28899–28910.
7 Y. Zhang, Y. Katayama, R. Tatara, L. Giordano, Y. Yu, D. Fraggedakis, J. G. Sun, F. Maglia, R. Jung, M. Z. Bazant and Y. Shao-Horn, *Energy Environ. Sci.*, 2020, **13**, 183–199.
8 B. L. D. Rinkel, J. P. Vivek, N. Garcia-Araez and C. P. Grey, *Energy Environ. Sci.*, 2022, **15**, 3416–3438.
9 A. R. Genreith-Schriever, C. S. Coates, K. Märker, I. D. Seymour, E. N. Bassey and C. P. Grey, *Chem. Mater.*, 2024, **36**, 4226–4239.
10 Y. Xia, J. Zheng, C. Wang and M. Gu, *Nano Energy*, 2018, **49**, 434–452.
11 H.-H. Ryu, K.-J. Park, C. S. Yoon and Y.-K. Sun, *Chem. Mater.*, 2018, **30**, 1155–1163.
12 A. R. Haworth, B. I. J. Johnston, L. Wheatcroft, S. L. McKinney, N. Tapia-Ruiz, S. G. Booth, A. J. Nedoma, S. A. Cussen and J. M. Griffin, *ACS Appl. Mater. Interfaces*, 2024, **16**, 7171–7181.
13 H. Banerjee, C. P. Grey and A. J. Morris, *Chem. Mater.*, 2024, **36**, 6575–6587.
14 H. Darjazi, E. Gonzalo, B. Acebedo, R. Cid, M. Zarrabeitia, F. Bonilla, M. Á. Muñoz-Márquez and F. Nobili, *Mater. Today Sustainability*, 2022, **20**, 100236.
15 P. Laine, M. Hietaniemi, J. Välikangas, T. Kauppinen, P. Tynjälä, T. Hu, S. Wang, H. Singh and L. Ulla, *Dalton Trans.*, 2023, **52**, 1413–1424.
16 J. Seo, J. Im, S. Yoon and K. Y. Cho, *Chem. Eng. J.*, 2023, **470**, 144406.
17 J. Im, J. Ahn, J. Y. Kim, E. J. Park, S. Yoon, Y.-G. Lee and K. Y. Cho, *Chem. Eng. J.*, 2022, **450**, 138159.
18 F.-M. Wang, E. B. Chemere, W.-C. Chien, C.-L. Chen, C.-C. Hsu, N.-H. Yeh, Y.-S. Wu, C. Khotimah, K. W. Guji

 This journal is © The Royal Society of Chemistry 2025

Published on 25 June 2025. Downloaded on 3/2/2026 11:28:34 PM.

and L. Merinda, *ACS Appl. Mater. Interfaces*, 2021, **13**, 46703–46716.
19 Y. Uchimoto, H. Sawada and T. Yao, *J. Power Sources*, 2001, **97–98**, 326–327.
20 M. G. Kim, N. E. Sung, H. J. Shin, N. S. Shin, K. S. Ryu and C. H. Yo, *Electrochim. Acta*, 2004, **50**, 501–504.
21 K. Kleiner, C. A. Murray, C. Grosu, B. Ying, M. Winter, P. Nagel, S. Schuppler and M. Merz, *J. Electrochem. Soc.*, 2021, **168**, 120533.
22 H. Huang, Y.-C. Chang, Y.-C. Huang, L. Li, A. C. Komarek, L. H. Tjeng, Y. Orikasa, C.-W. Pao, T.-S. Chan, J.-M. Chen, S.-C. Haw, J. Zhou, Y. Wang, H.-J. Lin, C.-T. Chen, C.-L. Dong, C.-Y. Kuo, J.-Q. Wang, Z. Hu and L. Zhang, *Nat. Commun.*, 2023, **14**, 2112.
23 Y. Ren, R. Yamaguchi, T. Uchiyama, Y. Orikasa, T. Watanabe, K. Yamamoto, T. Matsunaga, Y. Nishiki, S. Mitsushima and Y. Uchimoto, *ChemElectroChem*, 2021, **8**, 70–76.
24 N.-H. Yeh, F.-M. Wang, C. Khotimah, X.-C. Wang, Y.-W. Lin, S.-C. Chang, C.-C. Hsu, Y.-J. Chang, L. Tiong, C.-H. Liu, Y.-R. Lu, Y.-F. Liao, C.-K. Chang, S.-C. Haw, C.-W. Pao, J.-L. Chen, C.-L. Chen, J.-F. Lee, T.-S. Chan, H.-S. Sheu, J.-M. Chen, A. Ramar and C.-H. Su, *ACS Appl. Mater. Interfaces*, 2021, **13**, 7355–7369.
25 J. W. Freeland, M. Van Veenendaal and J. Chakhalian, *J. Electron Spectrosc. Relat. Phenom.*, 2016, **208**, 56–62.
26 G. Fu, X. Wen, S. Xi, Z. Chen, W. Li, J.-Y. Zhang, A. Tadich, R. Wu, D.-C. Qi, Y. Du, J. Cheng and K. H. L. Zhang, *Chem. Mater.*, 2019, **31**, 419–428.
27 A. O. Kondrakov, H. Geßwein, K. Galdina, L. De Biasi, V. Meded, E. O. Filatova, G. Schumacher, W. Wenzel, P. Hartmann, T. Brezesinski and J. Janek, *J. Phys. Chem. C*, 2017, **121**, 24381–24388.
28 C. Tian, D. Nordlund, H. L. Xin, Y. Xu, Y. Liu, D. Sokaras, F. Lin and M. M. Doeff, *J. Electrochem. Soc.*, 2018, **165**, A696–A704.
29 F.-M. Wang, T. Alemu, N.-H. Yeh, X.-C. Wang, Y.-W. Lin, C.-C. Hsu, Y.-J. Chang, C.-H. Liu, C.-I. Chuang, L.-H. Hsiao, J.-M. Chen, S.-C. Haw, W.-L. Chen, Q.-T. Pham and C.-H. Su, *ACS Appl. Mater. Interfaces*, 2019, **11**, 39827–39840.
30 F.-M. Wang, S.-C. Lo, C.-S. Cheng, J.-H. Chen, B.-J. Hwang and H.-C. Wu, *J. Membr. Sci.*, 2011, **368**, 165–170.
31 F.-M. Wang, C.-S. Cheng and J. Rick, *MRS Commun.*, 2012, **2**, 5–7.
32 Y. Cao, X. Liu, M. Kareev, D. Choudhury, S. Middey, D. Meyers, J.-W. Kim, P. J. Ryan, J. W. Freeland and J. Chakhalian, *Nat. Commun.*, 2016, **7**, 10418.
33 F.-M. Wang, *Polymers*, 2023, **15**, 2211.
34 T. Li, X.-Z. Yuan, L. Zhang, D. Song, K. Shi and C. Bock, *Electrochem. Energy Rev.*, 2020, **3**, 43–80.
35 P. Kuiper, G. Kruizinga, J. Ghijsen, G. A. Sawatzky and H. Verweij, *Phys. Rev. Lett.*, 1989, **62**, 221–224.
36 H.-M. Cheng, F.-M. Wang, J. P. Chu, B.-J. Hwang, J. Rick and H.-L. Chou, *J. Electrochem. Soc.*, 2017, **164**, A1393–A1400.